



# **Characterization of ultrashort mid-infrared femtosecond pulses using cross-correlation frequency resolved optical gating (XFROG)**

**Research Project Report**

by

**Stefan Schlauderer**

in the X-ray Femtochemistry and Cluster Physics Group at DESY (Hamburg)

under the supervision of Markus Jakob and Dr. Tim Laarmann

September 2015



# Contents

<b>1. Motivation</b>	<b>1</b>
<b>2. Theorie</b>	<b>2</b>
2.1. Characteristics of ultrashort laser pulses . . . . .	2
2.2. Pulse Shaping . . . . .	5
2.2.1. Programmable pulse shaper - the 4f line . . . . .	5
2.2.2. Acousto-optic modulator . . . . .	7
2.3. Characterization of ultrashort laser pulses . . . . .	8
<b>3. Experimental</b>	<b>11</b>
3.1. Laser system . . . . .	11
3.2. Pulse shaping . . . . .	11
3.3. The XFROG setup . . . . .	11
<b>4. Results</b>	<b>15</b>
<b>5. Summmary</b>	<b>17</b>
<b>References</b>	<b>18</b>

---

# 1. Motivation

Since the invention of the laser in 1966, there has been a steadily increasing interest from both the scientific as well as the industrial communities. Thereby, in the last few decades especially ultrashort laser pulses has been increasingly spotlighted due to their ability to reach very high peak intensities. Meanwhile light pulses are approaching durations of only one single cycle corresponding to no less than one to two femtoseconds ( $10^{-15}$ s) in the visible and near-infrared spectral region. As a result, ultrashort laser pulses have become crucial in various fields of research including the investigation and coherent control of ultrafast phenomena such as chemical reactions [Zwa00], magnetization dynamics [Big09] and many others [Die06]. This tremendous progress was spurred to a large extent by the breakthrough in the field of ultrafast pulse shaping, which enabled the generation of complex ultrafast waveforms according to user necessities [Wei00].

Strongly related to this field is the development of femtosecond pulse characterization techniques which enable the reconstruction of the spectral amplitude as well as the spectral phase of the pulse [Tre97, Iac98]. In order to verify theoretical models of pulse creation and to make even shorter pulses it is crucial to know all pulse properties in detail and to understand potential distortions that limit the length of currently available pulses [Har94][Chr95]. Moreover, it is always important to know at least the length of the pulse to determine the temporal resolution of the experiment. Despite this stringent necessity there was for a long time no technique which enabled the full characterization of ultrashort laser pulses. Fortunately, since Trebino et al. have invented the new pulse-measurement method frequency resolved optical gating (FROG) a remarkable progress has occurred. Nowadays, it is routine to fully characterize the time dependence of ultrashort laser pulses in the laboratory.

In this research project, a new setup for the temporal control and characterization of the electric field of femtosecond pulses with a center frequency in the mid-infrared spectral range is established. Thereby, the pulses are controlled in phase and amplitude by an acousto-optical modulator and completely characterized with the help of cross-correlation frequency resolved optical gating (XFROG).

## 2. Theorie

### 2.1. Characteristics of ultrashort laser pulses

Ultrashort laser pulses are electromagnetic wave packets, which can fully described by the space and time dependent electric field. Nevertheless, a complete characterization can be given either in the time or frequency domain. Neglecting the spatial and polarization dependence, the laser pulse can be described by its electric field [Die06]

$$\mathcal{E}(t) = \frac{1}{2}[E(t) + c.c.] \quad (2.1)$$

with the complex electric field in the time domain  $E(t) = E_0(t) \exp i\omega_0 t - \Phi(t)$  defined by a time dependent field amplitude  $E_0(t)$ , the center frequency  $\omega_0$  and the temporal phase  $\Phi(t)$  or by its field in the frequency domain

$$\tilde{\mathcal{E}}(\omega) = \frac{1}{2}[\tilde{E}(\omega) + \tilde{E}(-\omega)] \quad (2.2)$$

including the complex electric field  $\tilde{E}(\omega) = A(\omega) \exp i\phi(\omega)$  with the spectral amplitude  $A(\omega)$  and the spectral phase  $\phi(\omega)$ . However, as the temporal evolution of the electric field is not easy to access for ultrashort pulses, it is more convenient to use the spectral domain to characterize the pulse. Therefore, the shape of the pulse is fully given by the spectral amplitude  $A(\omega)$  and the spectral phase  $\phi(\omega)$ . The influence of the spectral phase on the shape of the femtosecond-pulse can be demonstrated by expanding  $\phi(\omega)$  as a Taylor series [Mon10]:

$$\phi(\omega) = \phi_0^{(0)} + \phi_0^{(1)}(\omega - \omega_0) + \frac{1}{2}\phi_0^{(2)}(\omega - \omega_0)^2 + \dots \quad (2.3)$$

with  $\phi_0^{(n)} = \frac{d^n \phi}{d\omega^n}|_{\omega_0}$ . Therefore,  $\phi_0^{(0)}$  is known as the absolute phase or rather the carrier envelope phase (CEP) (see figure 2.1), which plays an important role in nonlinear interactions like the high harmonic generation with few cycle pulses [Kra09].  $\phi_0^{(1)}$  corresponds to a delay between the pulse and an arbitrary initial point in time and leads to an constant group delay  $t_{group}(\omega)$ , which correspond to a temporal shift of the pulse in the time domain.  $\phi_0^{(2)}$  is the group delay dispersion, better known as *chirp* and has a rather vast effect on the pulse duration. Thus, each spectral component experiences a temporal delay that linearly increases (positive chirp) or decreases (negative chirp) with the angular frequency. This leads to an increase of the pulse duration. For a strong chirp, one can define the instantaneous frequency

$$\omega_{inst}(t) = \omega_0 - \frac{t}{\phi_0^{(2)}}. \quad (2.4)$$

Thus, for a positive chirped pulse, the instantaneous frequency increases linearly with time, whereas for a negative chirped pulse it decreases. If the pulse is *unchirped*, what means that the instantaneous frequency is constant, also the phase  $\phi(\omega)$  is constant. In this case, the shortest pulse duration is achieved and the pulse is said to be *Fourier limited*.

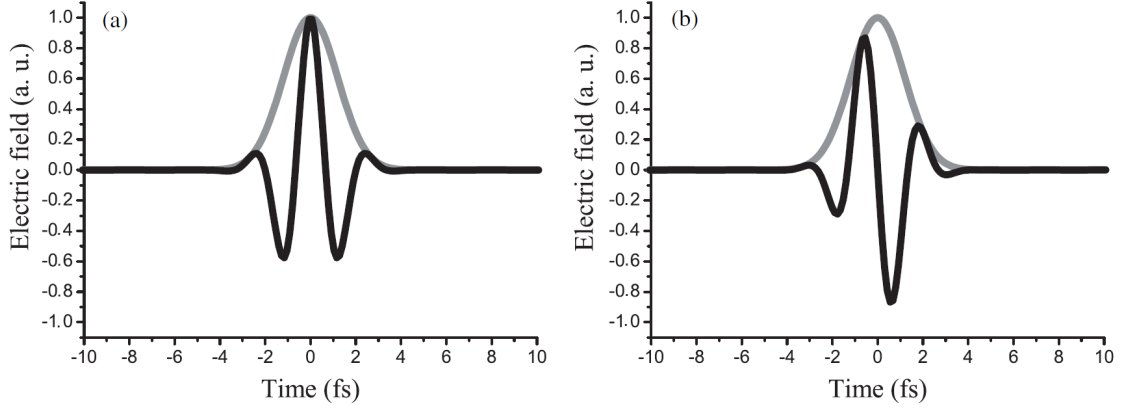


**Figure 2.1:** Ultrashort laser pulse with a central wavelength of 800 nm and a FWHM of 2 fs with two different carrier envelope phase: in (a), the electric field  $\mathcal{E}(t)$  (black) and the envelope (grey) show no absolute phase shift, the CEP is 0 rad, what results in a cosine pulse. In (b) the CEP is  $\frac{\pi}{2}$  what gives a sine pulse. From [Mon10].

In order to define the extent of the chirp one can use the time-bandwidth product (TBP)

$$TBP = \Delta t \Delta \omega \quad (2.5)$$

where  $\Delta t$  and  $\Delta \omega$  are the full-width at half maximum (FWHM) in intensity of the temporal and spectral profile of the pulse. The farther away from the Fourier limit, the stronger the chirp of the pulse.

To illustrate the influence of the particular components of the spectral phase and to visualize the shape of the femtosecond pulse, one can use either the spectral amplitude and phase (see figure 2.2 column 1) or the temporal intensity  $|E(t)|^2$  (see figure 2.2 column 2). However, the exact spatial and temporal location of these spectral components is hidden in the spectral phase. Wigner introduced a new two-dimensional representation of the electromagnetic wave packet, either in the plane of the space-wave vector or the time-angular frequency. The Wigner distribution of the complex temporal electric field  $E(t)$  can be written as [Pay92]

$$\mathcal{W}(t, \omega) = \int_{-\infty}^{+\infty} E(t + \frac{t'}{2}) E^*(t - \frac{t'}{2}) e^{-i\omega t'} dt' \quad (2.6)$$

or alternatively for the complex spectral electric field  $\tilde{E}(\omega)$

$$\mathcal{W}(t, \omega) = \frac{1}{2\pi} \int_{-\infty}^{+\infty} E(\omega + \frac{\omega'}{2}) E^*(\omega - \frac{\omega'}{2}) e^{-i\omega' t} d\omega'. \quad (2.7)$$

The two expressions can be transferred into each other by Fourier transform. In the third column of figure 2.2 the Wigner distribution function for different pulse shapes is shown. One can see that for rather common wave forms like a linear chirped pulse (figure 2.2 (b)), the Wigner distribution is a quite intuitive representation of the laser pulse. Nevertheless, if the complexity of the pulse increases, the interpretation of the Wigner distribution can be difficult. As an alternative, one can characterize the pulse with the help of its spectrogram

$$S(t, \omega) = \left| \int_{-\infty}^{+\infty} E(t') g(t' - t) e^{i\omega t'} dt' \right|^2. \quad (2.8)$$

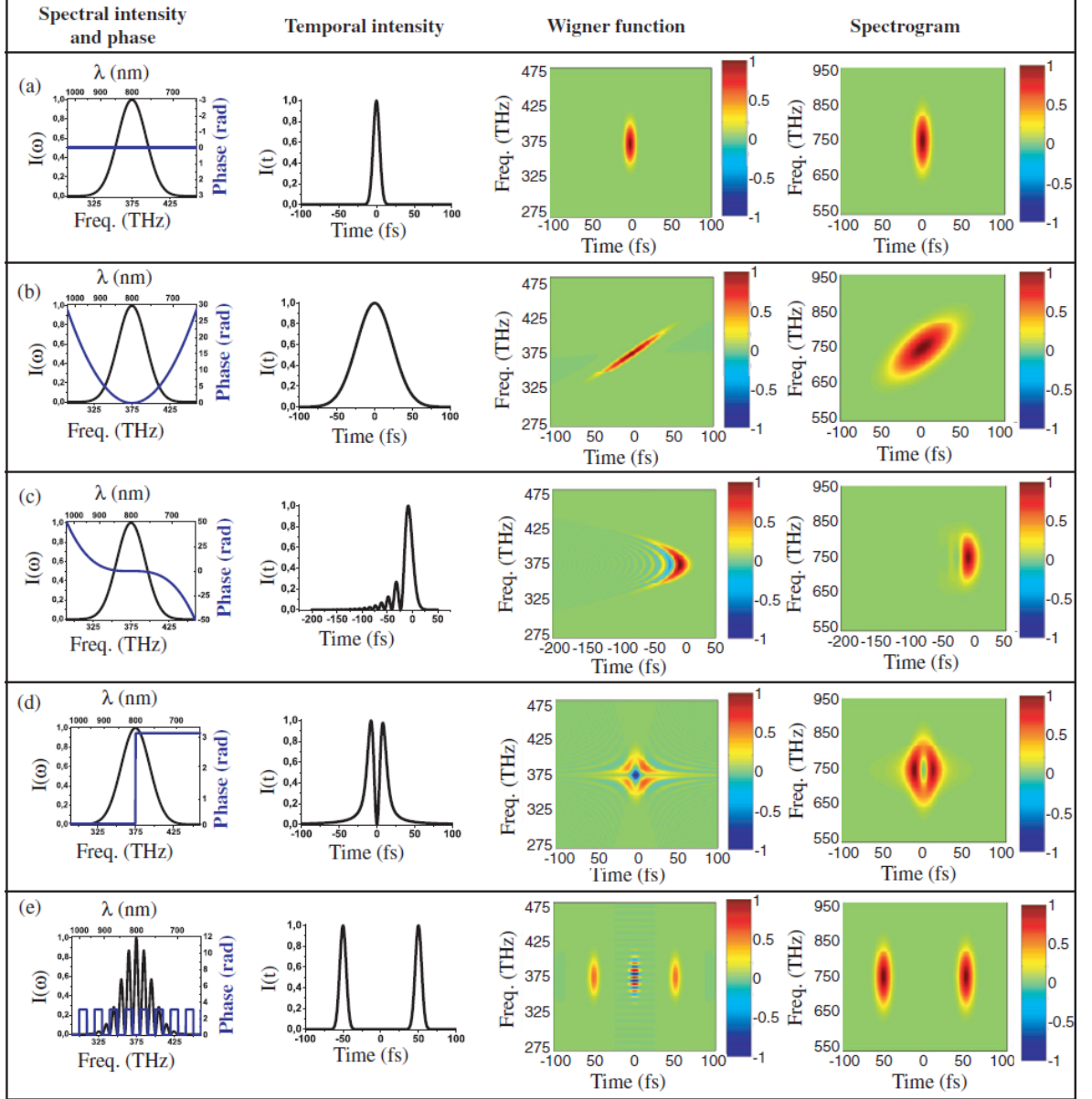


**Figure 2.2:** Gallery of pulses with different pulse shapes: (a) Fourier transform pulse, (b) chirped pulse, (c) cubic phase, (d) spectral  $\pi$ -jump, (e) two-pulse sequence. The first column shows the spectral intensity and phase, the second one the intensity vs. time, the third one the Wigner functions and the last one the spectrogram of the corresponding pulses. For the spectrogram, a Fourier limited 10 fs pulse at 800 nm was chosen as the gate. From [Mon10].

The spectrogram describes the temporal convolution of the electric field with a gate  $g(t)$ , what can be the pulse itself, and can be retrieved by special characterization techniques [Tre97]. The last column of figure 2.2 shows the spectrograms of the different generic pulses.

## 2.2. Pulse Shaping

In order to produce ultrafast optical waveforms according to user specifications, in the last few decades the field of ultrafast pulse shaping has been an active field of research. The big aim of this development is the programmable control of the amplitude, phase, frequency, polarization and/or the inter pulse separation of ultrashort laser pulses to control and guide dynamics on the ultrashort time scale. All existing pulse shaping techniques are based on a linear, time-invariant filter and can be expressed either in the time or spectral domain. Due to the difficulties of direct pulse shaping of femtosecond pulses, most devices are operating in the spectral domain. The electric field of the output pulse can then be expressed as follows [Tre14]:

$$\tilde{E}_{out}(\omega) = H(\omega)\tilde{E}_{in}(\omega). \quad (2.9)$$

$H(\omega)$  is called transfer function and describes the action of the pulse shaper on the incoming electric field  $\tilde{E}_{in}$ . However, all shaping techniques have only a certain capability. Thus, the shaping is restricted by the refresh rate  $R_{shape}$ , which is the time required to obtain a given waveform, the time shaping window  $T_{shape}$  and the spectral bandwidth of the pulse, which limits the variety of manipulable systems.

To manipulate the shape of ultrashort laser pulses, there is a variety of complex systems with extremely diverse range of usage. What type of technique is used depends on the user requirements. In the past decade, especially versatile pulse shaper based on programmable masks gained the interest of the scientific community. In the following chapter, one of the most common used setup, the zero-dispersion line or  $4f$ -line is introduced.

### 2.2.1. Programmable pulse shaper - the $4f$ line

As all programmable pulse shapers also the zero dispersion line modifies the spectral components by spatially separating them. Therefore, the  $4f$  line is composed of two diffraction gratings and two lenses with a focal length of  $f$  arranged in a  $4f$  set-up [Mon10]. By passing through the shaper, the spectral components of the incoming pulse are angularly dispersed by the first grating and then focused to small diffraction spots in the Fourier plane (FP) of the first lens. Thus, all spectral components are spatially separated and focused. By inserting a specific mask in the FP, it is possible to modify the optical path and/or the optical density of each spectral component separately. By doing so, one can control, depending on the mask, the phase, both phase and amplitude, the polarization as well as the inter pulse separation of the output pulse (see figure 2.3 (a)). The second combination of lens and grating allows the recombination of the different spectral components and collimates the beam again. Assuming a Gaussian input pulse in time and space with a central frequency  $\omega_0$  and the FWHM in intensity  $\Delta\omega_L$  in the spectral domain,  $\Delta t$  in the temporal domain



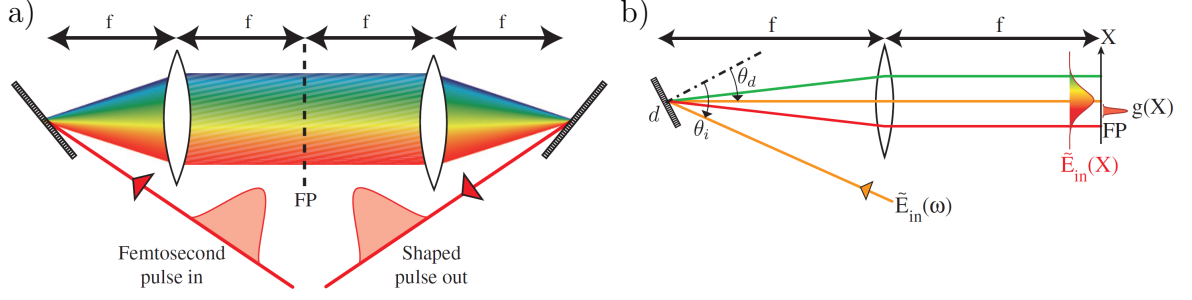


**Figure 2.3:** (a) Zero dispersion line composed of two gratings and 2 lenses organized in a  $4f$ -setup. Due to the first arrangement of grating and lens, the spectral components are spatially separated and focused in the Fourier plane (FP). After having passed the second arrangement, the outcome pulse is identical to the incoming pulse. (b) Half of a  $4f$ -line:  $\theta_i$  is the angle of incidence on the grating,  $d$  the grating period and  $\theta_d$  the diffraction angle of the spectral component at  $\lambda_0$ . The lens (focal length  $f$ ) maps the dispersed spectral components on the spatial coordinate  $X$  in the Fourier plane (FP).  $g(X)$  is the spatial extension of a given frequency component. From [Mon10].

and  $\Delta x_{in}$  in the spatial domain, one can specify the 4-line capabilities in shaping as follows [Dan89]:

According to figure 2.3 (b), the input pulse gets diffracted at the first grating (grating period  $d$ , focal length  $f$ ) by an angle of  $\theta_d$  at  $\lambda_0$ . Therefore, each spectral component has a finite size  $\Delta x_0$  in the Fourier plane. Introducing the spatial coordinate  $X$  in the FP, a frequency  $\omega_k$  is located at  $X_k$  given by

$$X_k = \alpha \omega_k \quad (2.10)$$

whereas  $\alpha$  is defined by the  $4f$ -line geometry:

$$\alpha = \frac{\lambda_0^2 f}{2\pi c d \cos \theta_d}. \quad (2.11)$$

Hence, the frequency resolution  $\delta\omega$  can be given as

$$\delta\omega = \frac{\Delta x_0}{\alpha}. \quad (2.12)$$

By Fourier transformation, this leads to the time shaping window

$$T_{shape} = \frac{4 \ln(2)}{\delta\omega} = \frac{\Delta x_{in}}{|v|} \quad (2.13)$$

with  $|v| = cd \cos \theta_i / \lambda_0$ . Formula (2.13) shows, that the time window for shaping  $T_{shape}$  is proportional to the input waist. This phenomena is known as spatio-temporal coupling. The reason for this correlation is simple: the first grating diffracts each frequency  $\omega$  into a certain direction  $k_\omega$ . The first lens maps  $k_\omega$  to the position  $X_\omega$  in the Fourier plane. Thus, the position  $X_\omega$  corresponds to a certain spectral component as well as to a certain direction. So the mask acting on the pulse at the position  $X_\omega$  modifies simultaneously  $\omega$  and  $k_\omega$ . This means, that for example in the case of a delay, the mask causes both a shift in time and along the transverse coordinate.

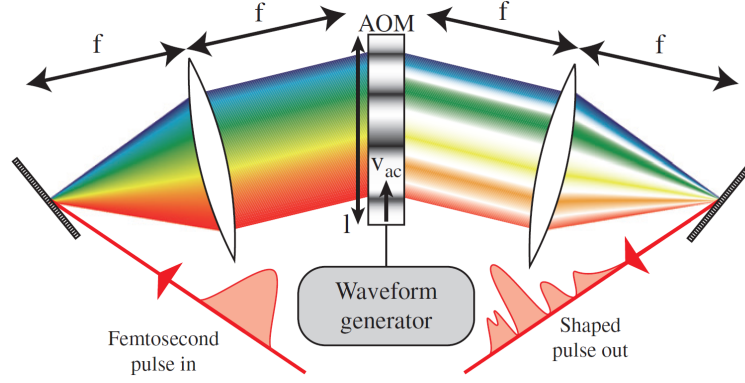


**Figure 2.4:** Programmable pulse shaper with an acousto-optic modulator (AOM) mask: the spatial mask pattern is generated by a temporal radio frequency voltage signal converted to a traveling acoustic wave in the AOM crystal, which acts on the incoming dispersed pulse like a refractive index grating.  $v_{ac}$  is the acoustic wave velocity,  $l$  the aperture of the AOM. From [Mon10].

As already mentioned, to turn the 4f-line into a pulse shaper, it is necessary to put a mask in its Fourier plane, where it acts simultaneously as spatial  $M_k$  and spectral mask  $M_\omega$ . In the following paragraph, the acousto-optic modulator (AOM) mask is described in greater detail.

### 2.2.2. Acousto-optic modulator

Using the technique of an acousto-optic modulator (AOM), the spatial pattern of the mask in the Fourier plane is derived from a temporal radiofrequency (RF) voltage signal, converted into a traveling acoustic wave by a piezoelectric transducer [Dug97]. Separated in space by the acoustic velocity  $v_{ac}$ , the spacial pattern in the AOM crystal acts as a refractive index grating with the grating period [Mon10]

$$\Lambda = \frac{v_{ac}}{\nu} \quad (2.14)$$

where  $\nu$  is the RF drive frequency. Through appropriate RF synthesis, the waveform of the incoming pulse can be modulated simultaneously in phase, amplitude and frequency. The resolution in either frequency and time domain is given by the ration of the crystal aperture  $l$  and the minimum acoustic-feature size. However, the used acousto-optic effect is based on a parametric interaction. Therefore, the efficiency of each diffraction order depends on the phase mismatch  $\delta_m$  between diffracted wave in the  $m$ -th order and the free acoustic and optical waves:

$$\delta_m \propto \Delta k_m L \propto Q \left( m - \frac{\sin \theta_0}{\sin \theta_B} \right) \quad (2.15)$$

with the Bragg angle  $\theta_B$  given by

$$\sin \theta_B = \frac{\lambda_0}{2n\Lambda}. \quad (2.16)$$

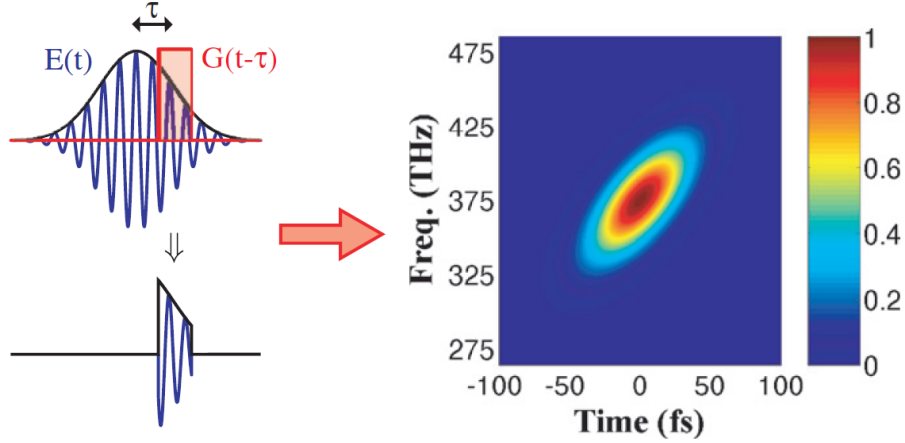


**Figure 2.5:** Principle of frequency resolved gating: The test pulse  $E(t)$  is sliced in time with the help of a gate pulse  $G(t - \tau)$ . The gated spectrum is measured as a function of the delay  $\tau$  between the gate  $G(t)$  and the test pulse. This yields a 2D spectrogram from which the spectral phase and amplitude can be retrieved using an iterative algorithm. From [Mon10].

$L$  is the thickness of the crystal,  $n$  the refractive index and  $\theta_0$  the incident angle of the optical wave on the AOM crystal.  $Q$  is a dimensionless parameter, used to classify the AOM regime [Mon10]:

$$Q = 2\pi \frac{L}{L_{eff}} = \frac{2\pi\lambda_0 L}{n\Lambda^2} \quad (2.17)$$

where  $L_{eff}$  is the effective interaction length. For  $Q \leq 0.1$ , which means  $L \ll L_{eff}$ , the AOM operates in the so called thin grating or Raman-Nath regime. In this case the best spatial resolution but only a limited efficiency of around 30% can be achieved. In the Bragg or thick grating regime ( $Q \geq 4\pi$ ,  $L \gg L_{eff}$ ) the laser is aligned at the Bragg angle and for the first-order phase matching is obtained. The diffraction efficiency can reach values up to 90%. In order to get a good compromise between efficiency and resolution it is common to operate the pulse shaping application at a  $Q$  value of  $Q = 4\pi$  [Dug97].

### 2.3. Characterization of ultrashort laser pulses

To predict the outcome of an experiment it is crucial to know the exact shape of the applied light pulse. Frequency variations during the pulse, known as chirp, for example can have a great impact on the rate of molecular photodissociation [Koh95]. However, due to the tremendous effort in generating ultrashort laser pulses with pulse durations down to a few femtoseconds, only incomplete characterization techniques like intensimetric autocorrelation or cross-correlation have been available for a long time. Using these devices it is indeed possible to reconstruct the intensity profile  $I(t)$  of the test pulse, but any information on the phase is not accessible. Thus, an overarching characterization of a short pulse should provide either the temporal electric field  $\mathcal{E}(t)$  or both the spectral amplitude  $A(\omega)$  and the spectral phase  $\phi(\omega)$  [Mon10]. This can be

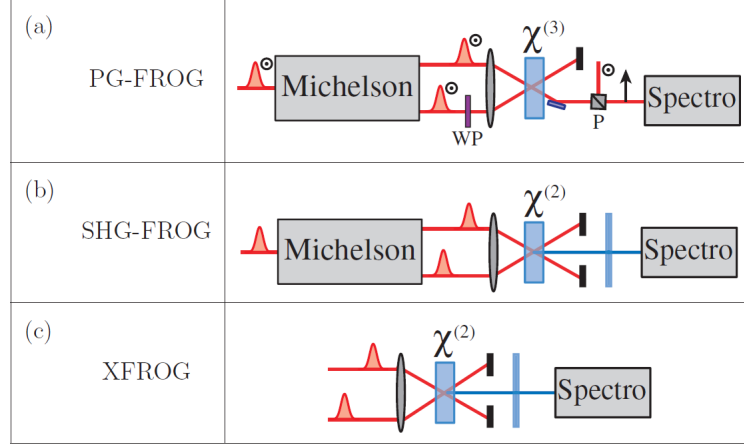


**Figure 2.6:** Schematic geometry of various FROG set-ups. (a) Polarization gating FROG (b) SHG FROG and (c) cross-correlation FROG. WP indicates the wave plate necessary to tune the polarization of the pulse, P is a polarization plate and  $\chi^2$  and  $\chi^3$  indicate the nonlinear susceptibilities of the crystal. From [Mon10].

done with so called self-referenced complete characterization methods like frequency resolved optical gating (FROG) as explained in the following.

### Frequency resolved optical gating (FROG)

Previously used techniques for characterizing ultrashort laser pulses operated either in the time or spectral domain. Spectrometers for example operate in the spectral domain and measure the spectrum or more specifically the spectral amplitude  $A(\omega)$ , but can not access the spectral phase of the pulse. In the time domain using autocorrelators and the pulse itself as reference, it is possible to measure a smeared out version of  $I(t)$ . However, there are several unknown parameters, which enable only a guess of the real pulse shape. Using frequency resolved optical gating (FROG) to characterize the pulse, it is possible to retrieve the pulse shape with essentially temporal infinite time and spectral resolution [Tre97]. This can be achieved by operating simultaneously in the time as well as in the frequency domain. This enabled the measurement of extremely short laser pulses with durations down to only a few femtoseconds.

The main idea of FROG is to temporally gate the test pulse  $E(t)$  with a reference pulse  $G(t)$  and then measuring the spectrum of this gated pulse as a function of the delay  $\tau$  between the test and the gate pulse. This gives a 2D signal, known as the spectrogram of the pulse

$$S(\tau, \omega) = \left| \int_{-\infty}^{\infty} E(t) G(t - \tau) e^{-i\omega t} dt \right|^2 \quad (2.18)$$

which is sufficient to completely determine  $E(t)$  [Tre97]. As there is no shorter pulse available than the pulse itself, like in an intensimetric autocorrelator, a nonlinear process has to be used for gating. As there are several beam geometries imaginable, a whole zoo of FROG techniques exists. The maybe most common used method is based on second-harmonic generation, whereas the gate pulse is simply a time-delayed replica of the test pulse [DeL94]. However, in the following the cross-correlation frequency resolved optical gating (XFROG) geometry is explained in more detail. In combination

with the fast iterative retrieval algorithm developed by Kane et al. [Kan99] it is possible to determine simultaneously the gate and the test pulse. Therefore, this technique is particularly suited for the characterization of strongly shaped pulses using a small fraction of the pump pulse as gate pulse  $E_G(t)$  for the pulse characterization. In doing so, the spectrogram detected by the spectrometer takes the form

$$S^{XFROG}(\tau, \omega) \propto \left| \int_{-\infty}^{\infty} \chi^{(2)} E(t) E_G(t - \tau) e^{i\omega t} dt \right|^2 = \left| \int_{-\infty}^{\infty} E_{sig}(t, \tau) e^{i\omega t} dt \right|^2 \quad (2.19)$$

with the autocorrelator signal field

$$E_{sig}(t, \tau) = \chi^{(2)} E(t) E_G(t - \tau) \quad (2.20)$$

which depends in the case of XFROG technique on the nonlinear susceptibility  $\chi^{(2)}$  as sum-frequency generation in a nonlinear crystal is used to gate the test pulse.

Equations (2.19) and (2.20) depict the boundary conditions, which have to be satisfied by solving following equation for the phase  $\phi(\omega, t)$  [Kan99]:

$$\sqrt{S^{XFROG}(\tau, \omega)} \phi(\omega, t) \propto \left| \int_{-\infty}^{\infty} \chi^{(2)} E(t) E_G(t - \tau) e^{i\omega t} dt \right|. \quad (2.21)$$

Now, the developed fast retrieval algorithm by Kane et al. uses a special iteration technique, which utilizes fast Fourier-transformation to switch between frequency and time domain in order to find a self-consistent solution of this two-dimensional phase retrieval problem for ultrashort laser pulses. As the spectral amplitude  $A(\omega)$  can be derived directly from the spectrogram  $S(\tau, \omega)$ , this yields to a full characterization of the pulse.

---

### 3. Experimental

In the following the main components of the new setup, the laser system, the acousto-optic pulse shaper and the XFROG setup are described in greater detail.

#### 3.1. Laser system

Within this research project a commercial laser system from *LIGHT CONVERSION* is used, which consists of a Yb:KGW laser oscillator with a regenerative amplifier and an optical parametric amplifier. The fundamental of the laser oscillator has an output wavelength of about 1030 nm, a repetition rate of 5 kHz, a pulse duration down to 150 fs and a maximum pulse energy of up to 1 mJ. Using a pellicle beamsplitter about 80% of the output beam are guided into the OPA whereas the other 20% are directly lead to the experiment. The optical parametric amplifier enables a broad range of wavelength conversion ranging from 600 to 2720 nm, whereas the used idler beam can be tuned from 900-2720 nm. To get ideal makings, the idler is adjusted to 2102 nm, having a pulse energy of 1,14  $\mu$ J [LIG14].

#### 3.2. Pulse shaping

To shape the mid-infrared pulse with a centre frequency of 2102 nm, an acousto-optical modulator mask (see chapter 2.2.2) is used. Thereby, the pulse shaper consists of two diffraction gratings with 75 lines/mm and two ZnSe lenses with a focal length of  $f = 200$  mm arranged in a  $4f$ -setup. The spatial mask patten is generated by a temporal radio frequency voltage signal converted to a travelling acousto-optical wave in the germanium monocrystal, used as AOM crystal. The pulse shaper is tunable from 2-15  $\mu$ m.

#### 3.3. The XFROG setup

AS mentioned in the previous chapter, by using frequency resolved optical gating it is possible to fully characterize any ultrashort laser pulse with a duration of down to only a few femtoseconds. This is done by simply spectrally resolving the signal beam of an autocorrelator. Therefore one obtains additional informations about the shape of the nonlinear signal which serves as boundary condition for the reconstruction of the pulse. Using the beam geometry of XFROG it is possible to retrieve both the test as well as the gate pulse. However, the main reason for using this specific setup for our purpose is the centre frequency od the used test pulse in the mid-infrared spectral range. The most common used spectrometers, based on silicon detectors, are insensitive to infrared light. Therefore, it appears reasonable to use the nonlinear process of sum-frequency generation convert the pulses to the visible regime. In our case this is done by mixing the fundamental of the laser oscillator at 1030 nm with the mid-infrared, shaped idler pulses at 2102 nm. This leads to a sum-frequency of 691.3 nm which can be easily detected with the available spectrometer.

Figure 2.6 illustrates the established XFROG setup, whose optimization and setup was the main task of this research project. XFROG works easily spoken like a spectrally

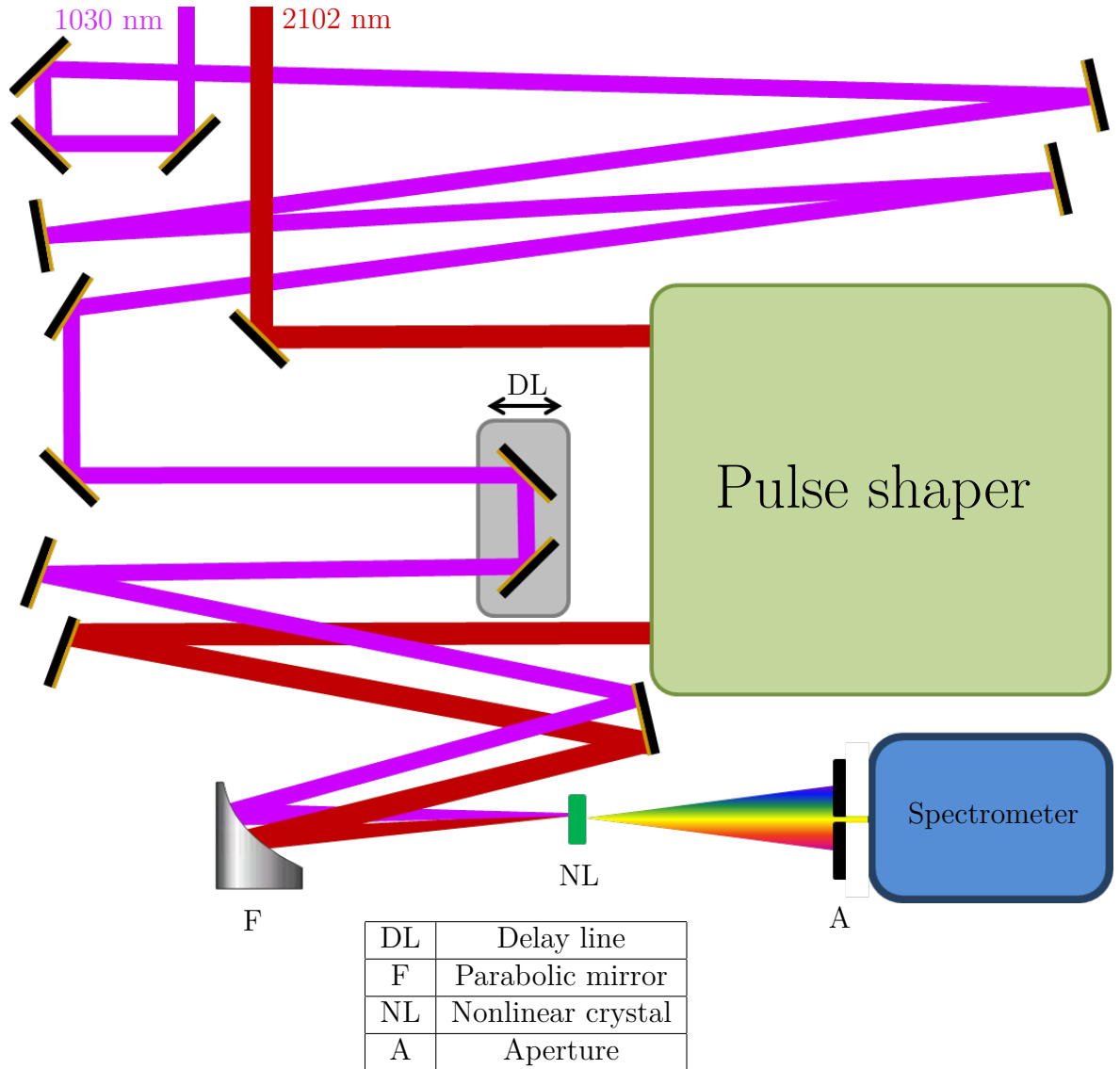


**Figure 3.1:** Schematic geometry of the established XFROG-Setup. To ensure temporal overlap of the two pulses, the beam path of the gate pulse (1030 nm) is folded. With the help of the delay line (DL) the gate pulse can be delayed versus the test pulse (2102 nm), which is lead through the pulse shaper. Both pulses then are focussed into the nonlinear crystal (NL) by the focusing mirror(F). There, they are superimposed and according to the nonlinear process of sum-frequency generation, a spectral component is generated, which easily can be detected by the spectrometer. Due to the phase matching condition, the generated beam is spatially separated from the test and gate pulse and can therefore be isolated with the help of the aperture (A).

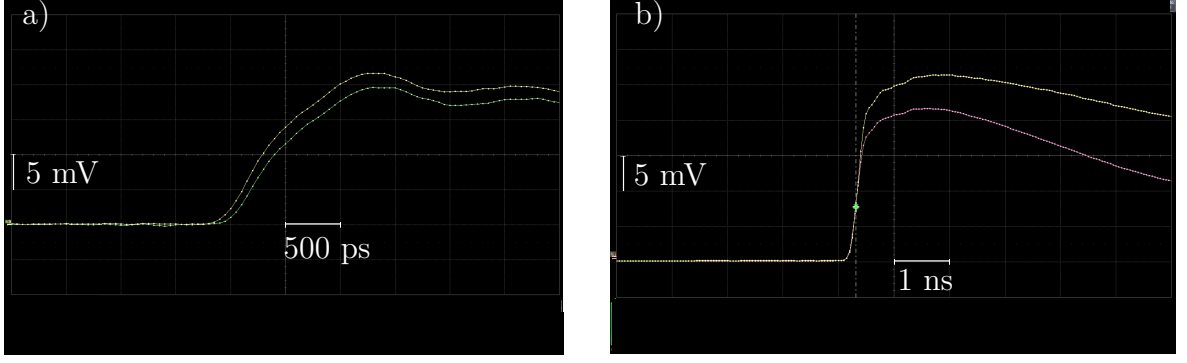


**Figure 3.2:** Adjustment of temporal overlap by measuring the arrival times of the gate and test pulse by using a ultra fast photodiode and a oscilloscope with a bandwidth of 2.5 GHz and a sampling rate of 20 GS/s: (a) Before the fine adjustment of the optical components, there is a temporal delay of 105 ps between the gate (yellow) and test (green) pulse. (b) By readjusting one of the mirror, this delay could be reduced down to the resolution limit of the spectrometer (yellow: gate pulse, red: test pulse).

resolved autocorrelator. Therefore it is essential to have perfect temporal and spatial overlap of the test (2102 nm) and gate (1030 nm) pulse. The mid-infrared beam has due to the propagation through the OPA a much longer beam path. Therefore, it is necessary to temporarily delay the 1030 nm beam to get temporal overlap. This is done by folding the beam path of the gate pulse so much so that both beams have the same length to pass. Using a high speed photodiode with a rise time shorter than 1 ns and an oscilloscope of *LeCroy* with a bandwidth of 2.5 GHz and sampling rate of 20 GS/s which corresponds to a temporal resolution of 100 ps, the perfect temporal overlap is determined. Figure 3.2 (a) shows the oscillogram of the two pulses, using a independent trigger signal, which originates from a leakage signal of the regenerative amplifier. One can observe a temporal offset of 105 ps which means a path difference of 3.15 cm. After readjusting the optical components, this offset could be reduced down to the resolution limit of the oscilloscope (see figure 3.2 (b)). The variable delay line (DL) is controlled by a custom written *LabVIEW* VI and has a range of 1 inch (2.54 cm) what corresponds to a delay of  $\pm 86$  ps. Hence, the delay line can be used to adjust the perfect temporal overlap and allows to temporally delay the gate pulse versus the test pulse.

With a focusing mirror (F) the two beams are then focused in the nonlinear crystal (NL), where the sum-frequency of the 2102 nm- and 1030 nm-pulse is generated. To guarantee the spatial overlap of the two pulses, the position of the foci was pinpointed with the help of a pinhole with a diameter of 100  $\mu\text{m}$ . The spotsize of the 1030 nm beam was calculated to be 52.5  $\mu\text{m}$ , that of the 2102 nm beam is 107.1  $\mu\text{m}$ .

Due to the high damage threshold and high effective nonlinearity ( $d_{eff} = 1,98 \frac{\text{pm}}{\text{V}}$ ) a beta-barium borate (BBO) crystal is used as nonlinear crystal. To fulfill the phase matching condition and to ensure maximal conversion efficiency for the nonlinear process

$$2102 \text{ nm } (o) + 1030 \text{ nm } (o) \rightarrow 691,3 \text{ nm } (e) \quad (3.1)$$

the mid-infrared and the 1030 nm-pulse have to be polarized perpendicular to the optical axis (ordinary (o)), whereas the generated beam is polarized parallel (extraordinary



(e)) with respect to the optical axis . The nonlinear crystal is cut in an angle of  $\theta = 20^\circ$  to the optical axis. Due to the phase matching condition for the wave vectors

$$\vec{k}_{2102nm} + \vec{k}_{1030nm} = \vec{k}_{691,3nm} \quad (3.2)$$

and the non-collinear superimposition of the incoming beams, the generated beam can be found between the two incoming beams and is thus spatially separated from them. Using a spectrometer with spectral sensitivity ranging from 200 nm 850 nm, the spectral intensity of the sum-frequency signal is detected for various delays  $\tau$  of the gate pulse. As a result, this yields the spectrogram, what can be used, together with the iterative algorithm explained in chapter 2.3, to retrieve the spectral phase and amplitude of the test pulse.

## 4. Results

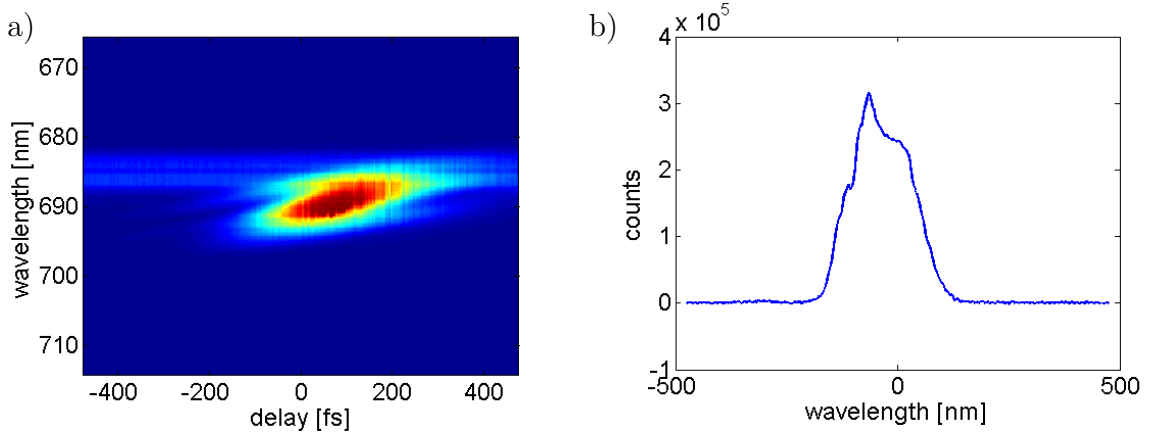


**Figure 4.1:** Measured FROG trace. (a) Spectrogram of the test pulse, measured in 256 steps over a range of 948 fs. One can see that the pulse is positively chirped and has a center frequency of  $\approx 691$  nm. With the help of the profile of the pulse, see (b) one can estimate the pulse duration (FWHM) to 167.4 fs.

The major task of this research project is the optimization and the establishment of a XFROG setup. However, after the adjustment of the perfect temporal and spatial overlap, it was possible to detect the first FROG traces with the new setup. To get a sufficient spectrogram of the test pulse, a temporal range of 948 fs is scanned with a resolution of 3.7 fs. The used spectrometer has a wavelength spacing of 0.19 nm. The resulting 2D map of the unshaped 2102 nm-pulse is shown in figure 4.1 (a). One can see that the mid-infrared pulse is positively chirped, as the instantaneous frequency of the pulse is increasing with time. Moreover, by plotting the cross profile of the pulse (see figure 4.1 (b)), one can estimate the pulse duration and the central frequency of the pulse. The pulse duration (FWHM) is approximately 167.4 fs, where the central frequency is about 691 nm, which are both reasonable values according to the output wavelength of the laser oscillator of  $\approx 160$  fs and formula (3.1), which defines the nonlinear process of sum-frequency generation.

Now, using the iterative algorithm developed by Trebino and co-workers [Kan99], one can start with the reconstruction of the mid-infrared test pulse. To analyze the spectrogram, the *MATLAB* code needs either a  $256 \times 256$  or  $512 \times 512$  array. To do so, the relevant spectral and temporal range including the sum-frequency signal are selected (see figure 4.2 (a)) and fed into the algorithm. To completely retrieve the shape of the test pulse, it is necessary to specify the gate pulse. As the 1030 nm-pulse is not characterized yet, this first pulse reconstruction is done with an ideal Gaussian gate pulse with a central wavelength of 1030 nm and a FWHM of 160 fs generated with the help of the pulse generator implemented in the Trebino algorithm (see figure 4.2 (b)). Figure 4.3 shows the resulting reconstructed pulse, which already can be retrieved with quite a high precision. However, due to the idealistic gate pulse and also some artifacts originating from the Fourier transformations, the central wavelength and also the pulse duration could not be determined properly yet. So further characterization of the real gate is necessary.

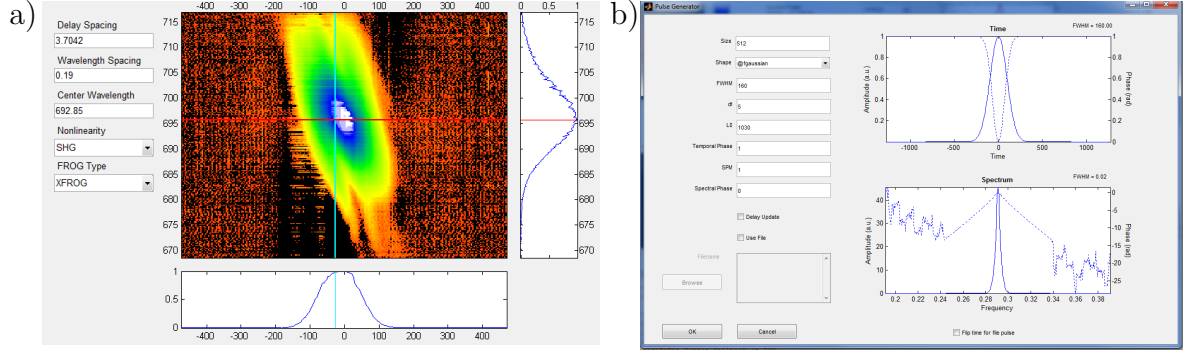


**Figure 4.2:** Input for the reconstruction of the test pulse. (a) FROG trace of the test pulse measured with a temporal resolution of 3.7 fs and a wavelength spacing of 0.19 nm. The center wavelength of the detected spectrogram is 692.85 nm. (b) Interface of the pulse generator implemented in the used retrieval algorithm. To reconstruct the spectral phase of the mid-infrared pulse, an ideal Gaussian pulse with FWHM 160 fs and a central wavelength of 1030 nm is generated.

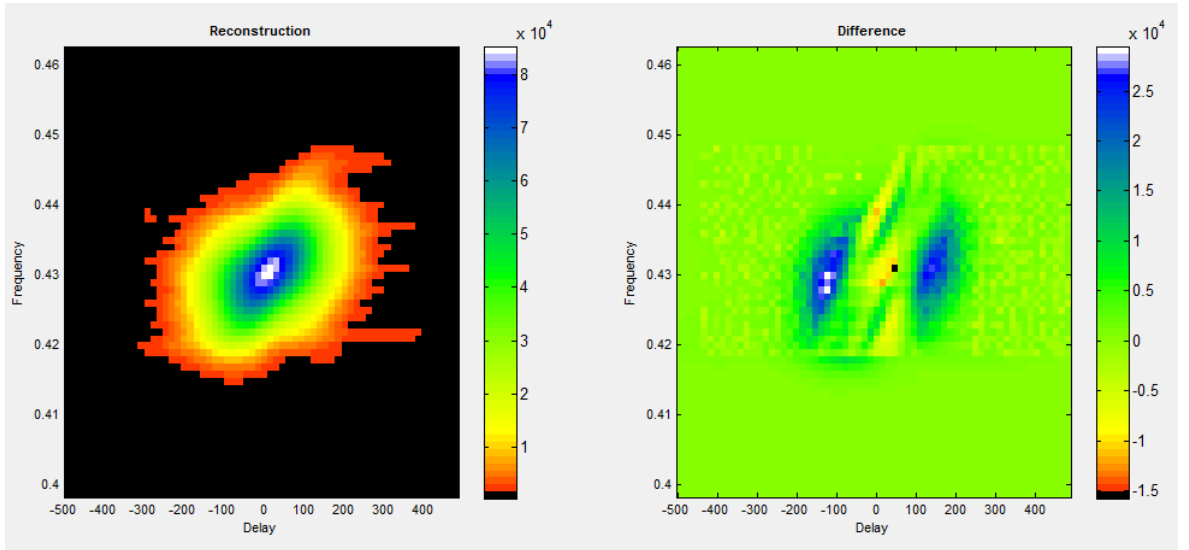


**Figure 4.3:** Reconstructed pulse. Using the retrieval algorithm developed by Trebino et al. [Kan99] it is possible to retrieve the shape of the mid-infrared test pulse with very high precision. However using the gate pulse shown in figure 4.2 (b), the correct center wavelength and pulse duration could not be retrieved yet. Therefore, further characterization of the real gate pulse is necessary.

---

## 5. Summary

In this work a new XFROG setup, which enables the overarching characterization of ultrashort laser pulses, has been optimized and established. The setup is designed to specifically determine the pulse shape of pulses in the mid-infrared, whose spectral components can be manipulated with the help of a pulse shaper using an acousto-optical modulator mask where appropriate.

For this purpose the idler of the OPA is adjusted to 2102 nm. This mid-infrared beam is then superimposed with the fundamental of the Yb:KGW laser oscillator, which has a central wavelength of 1030 nm. Fulfilling the phase matching condition for sum-frequency generation, it is then possible to generate spectral components in the visible range, which easily can be detected with the help of a spectrometer. However, the sum-frequency of the test (mid-infrared) and the gate (1030 nm) pulse is only generated when the two pulses are perfectly temporal and spatial overlapping. Therefore the temporal overlap has been adjusted coarsely with the help of an ultrafast photodiode and an oscilloscope with a bandwidth of 2.5 GHz and a sampling rate of 20 GS/s, which corresponds to a temporal resolution of 100 ps. Using a motorized delay stage controlled by a custom written *LabVIEW* program, the perfect temporal overlap could be established. Moreover, this enables to temporally delay the gate pulse versus the test pulse with a resolution of only a few femtoseconds. The spatial overlap was achieved by pinpointing the position of the foci with the help of a pinhole with a diameter of 100  $\mu\text{m}$ . Detecting a spectrum for each delay step it was then possible to detect the first spectrogram of the mid-infrared pulse with a resolution of 3.7 fs. Using the iterative retrieval algorithm developed by Trebino and co-workers, the spectrogram can be used to reconstruct the exact shape of the test pulse. The central wavelength of the FROG trace is approximately 691 nm. The pulse duration could be estimated to 167.4 fs. However, as it has not been possible to fully characterize the gate pulse yet, an idealistic gate pulse was used for the reconstruction. Because of that and also due to some artifacts originating from the Fourier transformations, the reconstructed pulse does not reflect the real pulse shape of the mid-infrared test pulse.

Nevertheless, in the future, after having optimized the pulse retrieval algorithm, it will be possible to fully characterize ultrafast laser pulses up to a central wavelength of 15  $\mu\text{m}$  with the help of the novel XFROG setup. Furthermore, these pulses can be controlled in spectral amplitude and phase using the AOM pulse shaper. This will pave the way to a variety of applications in molecular science like the optical excitation, control and observation of an electronic charge transfer in an ongoing chemical reaction.

## References

- [Big09] Jean-Yves Bigot, Mircea Vomir, and Eric Beaurepaire, *Coherent ultrafast magnetism induced by femtosecond laser pulses*, Nature Physics **5**, 515–520 (2009).
- [Chr95] I P Christov, H C Kapteyn, M M Murnane, C P Huang, and J Zhou, *Space-time focusing of femtosecond pulses in a Ti:sapphire laser.*, Optics letters **20**, 309–311 (1995).
- [Dan89] M B Danailov and I P Christov, *Time-space Shaping of Light Pulses by Fourier Optical Processing*, Journal of Modern Optics **36**, 725–731 (1989).
- [DeL94] K. W. DeLong, Rick Trebino, J. Hunter, and W. E. White, *Frequency-resolved optical gating with the use of second-harmonic generation*, Journal of the Optical Society of America B **11**, 2206 (1994).
- [Die06] Jean-Claude Diels and Wolfgang Rudolph, *Ultrashort Laser Pulse Phenomena*, Elsevier, 2006.
- [Dug97] M. a. Dugan, J. X. Tull, and W. S. Warren, *High-resolution acousto-optic shaping of unamplified and amplified femtosecond laser pulses*, Journal of the Optical Society of America B **14**, 2348 (1997).
- [Har94] J D Harvey, J M Dudley, P F Curley, C Spielmann, and F Krausz, *Coherent effects in a self-mode-locked Ti:sapphire laser.*, Optics letters **19**, 972–974 (1994).
- [Iac98] C Iaconis and I a Walmsley, *Spectral phase interferometry for direct electric-field reconstruction of ultrashort optical pulses.*, Optics letters **23**, 792–794 (1998).
- [Kan99] D.J. J Kane, *Recent progress toward real-time measurement of ultrashort laser pulses*, IEEE Journal of Quantum Electronics **35**, 421–431 (1999).
- [Koh95] Bern Kohler, Vladislav V Yakovlev, Jianwei Che, Jeffrey L Krause, Michael Messina, Kent R Wilson, Nikolaus Schwentner, Robert M Whitnell, and Yi-Jing Yan, *Quantum Control of Wave Packet Evolution with Tailored Femtosecond Pulses*, Physical Review Letters **74**, 3360–3363 (1995).
- [Kra09] Ferenc Krausz and Misha Ivanov, *Attosecond physics*, Reviews of Modern Physics **81**, 163–234 (2009).
- [LIG14] LIGHT CONVERSION, *LIGHT CONVERSION Service Report SR PHAROS & ORPHEUS*, Tech. report, 2014.
- [Mon10] Antoine Monmayrant, Sébastien Weber, and Béatrice Chatel, *A newcomer’s guide to ultrashort pulse shaping and characterization*, Journal of Physics B: Atomic, Molecular and Optical Physics **43**, 103001 (2010).
- [Pay92] J. Paye, *The chronocyclic representation of ultrashort light pulses*, IEEE Journal of Quantum Electronics **28**, 2262–2273 (1992).

- [Tre97] Rick Trebino, Kenneth W. DeLong, David N Fittinghoff, John N Sweetser, Marco a. Krumbügel, Bruce a Richman, and Daniel J Kane, *Measuring ultrashort laser pulses in the time-frequency domain using frequency-resolved optical gating*, Review of Scientific Instruments **68**, 3277 (1997).
- [Tre14] Rick Trebino, *Ultrafast Optics Course*, 2014.
- [Wei00] a. M. Weiner and I Introduction, *Femtosecond pulse shaping using spatial light modulators*, Review of Scientific Instruments **71**, 1929 (2000).
- [Zwa00] Ahmed H Zwail, *Femtochemistry:Atomic-Scale Dynamics of the Chemical Bond*, The Journal of Physical Chemistry A **104**, 5660–5694 (2000).